Parameter investigation of the experimental methodology of electrical conductivity measurements for PbO containing slags

Pieter-Jan Boeykens[a], Inge Bellemans[a], Lennart Scheunis[b], Kim Verbeken[a]

[a] Department of Materials, Textiles and Chemical Engineering, Ghent University, Research group Sustainable Materials Science Technologiepark 46, Zwijnaarde (Ghent), 9052 Belgium

[b] Umicore N.V., Umicore Research & Development, Watertorenstraat 33, Olen, 2250 Belgium

Corresponding author: Kim Verbeken

E-mail adress: kim.verbeken@ugent.be

Adress: Department of Materials, Textiles and Chemical Engineering, Ghent University, Research group Sustainable Materials Science Technologiepark 46, Zwijnaarde (Ghent), 9052 Belgium

Keywords:

Pyrometallurgy

Lead silicate slags

Electrical conductivity

Four-electrode measurement setup

Impedance measurements

Abstract

During pyrometallurgical extraction, some metals are lost to the slag phase which limits the process efficiency and may also cause environmental harm if those slags are used afterwards for the concrete industry. One way to reduce metal losses is via slag cleaning in a submerged arc electric furnace (SAF) where heat is generated via the conversion of electricity via the slag's resistance and thus the slag's electrical conductivity is an important process parameter. To study this parameter, a four-electrode conductivity setup was constructed as it can provide equally fast results as a two-electrode configuration but without the need for a cable correction as this correction may introduce measurement errors. To make a comparison between both setups, a binary SiO_2-PbO system was tested as this system has already been frequently studied via two-electrode setups in literature. Our experimental data and activation energy values agree with those from literature which confirms that our setup provides reliable data. In addition, specific focus was put on the experimental methodology in terms of reproducibility, measurement technique (Electrochemical Impedance spectroscopy (EIS) versus single frequency measurements) and crucible materials (Pt-Ir versus Al_2O_3). The standard deviation on our results is found to be within the same range as those in literature. EIS and the single frequency method yields the same results with the difference being less than 1%. Finally, the crucible material has a clear influence as the oxidic crucible increases the cell constant by a factor 3 compared to a metallic crucible. The resulting conductivity values for the liquid PbO-SiO_2 slags are of similar order, but the measurements in Al_2O_3 are unstable over time as the conductivity decreases continuously during the experiment due to crucible dissolution.

1. Introduction

It is expected that metal demands will continue increasing in the 21st century, while metal ores obtained via mining are expected to either decrease in quality or become more and more depleted [1–3]. Hence, in order to ensure future needs, it is necessary to focus on both metals recycling as well as on increasing the efficiency of current extraction technologies. One of the first steps of this extraction process is the melting and subsequent separation of the metals from gangue ore/impurities at high temperatures (> 1000 °C). Within this pyrometallurgical step, the impurities are typically collected in a slag (metal oxide) phase which floats on top of a liquid metal or liquid matte (metal sulphides) phase [4]. After a sufficient amount of metal/matte is produced, the slag phase will be tapped from the furnace and either sent towards land filling or used within the construction industry [5,6].

Unfortunately, this metal-slag separation is typically incomplete and metal is still present within the slag phase with metal contents up to 20-25% for steel and up to 10% for non-ferrous metal production [7,8]. Hence, this limits the process efficiency, which induces economic losses, but also results in environmental damage as these metals may leach out causing soil pollution [5]. Metal losses are typically categorized as either chemical or mechanical [8,9].The first type signifies the presence of the metal being present as a metal oxide or sulphide in the slag phase, which is intrinsically linked to the thermodynamics of the smelting process [8]. On the other hand, the second loss is due to metal droplets being entrained in the slag which is related to the furnace operation. These droplets have several potential origins as metal can become trapped in the slag during furnace charging or slag tapping, via gas bubbles passing the metal/matte-slag interface or via chemical precipitation within the slag due to chemical reactions or temperature/oxygen level gradients [7]. In addition, these droplets may not

be recovered during sedimentation as they may stick to solid particle present in the slag, such as magnetite/spinel phases. As these metal droplet – solid entity has a density lower than that of the metal itself, these entities will not be collected within the metal phase as they are trapped just above the liquid metal [8].

From the above, it becomes clear that an additional process step is required to recover these metals from the slag phase which is known as slag cleaning. One way to do this is via the Submerged Electric Arc Furnace (SAF), in which the current carrying electrodes are submerged within the liquid slag [9]. In this furnace, metal oxides are reduced to metals via adding a reductant such as coke, while the metal droplets are allowed to coalesce and eventually settle at the bottom of the furnace. The droplet settling rate can be increased via decreasing the slag's viscosity which can be achieved via increasing the temperature. In addition, the increase in temperature and reducing atmosphere may lead to the dissolution of solids so that droplets are no longer attached to the solids and hence trapped. Heat in this furnace is generated via Joule heating, which is the conversion of the imposed electric current to heat using the slag's electrical resistance according to Equation (1). Herein, P is defined as the power (W), *I* is the current (A) and *R* the slag's resistance (Ω) [10]. The slag's resistance itself is inversely proportional to the slag's electrical conductivity σ (S/cm) and linearly proportional to the furnace's cell constant *G* (cm^{-1}), which is dependent on the electrode geometry and placement within the furnace [11].

$$P = I^2 R = I^2 \frac{G}{\sigma} \quad (1)$$

From Equation (1), it is evident that the slag's electrical conductivity is an essential material property for a proper furnace operation. This is further complemented by Computational Fluid Dynamics (CFD) simulations carried out by Karalis et al.[12] as a

function of the slag's electrical conductivity. This study showed that small variations for this parameter lead to significant changes in the furnace's temperature profile. Thus, in order to dimension and operate a SAF, accurate electrical conductivity values and thus also measurements are needed. However, electrical conductivity measurements can be done via multiple setup types and measurement techniques, with none of them defined as a standardized one. In addition, experimental data for the same slag composition from different authors may significantly differ from each other [13,14]. As such, a first goal of this study is to provide an overview of different measurement setups and techniques. As a second goal, an experimental methodology was developed to perform electrical conductivity measurements with PbO containing slags. For this, a dedicated setup was constructed (inspired by the prototype setup in[15]) and it is verified similarly with a simple binary SiO_2 – PbO slag system. Finally, specific attention is drawn to the crucible material used for performing experiments.

2. Electrical conductivity measurements

2.1. Measurement procedure

Before explaining the different types of available setups, it is first necessary to look at the basic definition of the electrical conductivity and how this property can be measured. The electrical conductivity of a material is a measure for the ability of a material to conduct an electrical current. Unfortunately, the electrical conductivity of a material cannot be measured directly and needs to be derived from the resistance. The relationship between the electrical conductivity σ ($S.cm^{-1}$) and the resistance R (Ω) is defined according to Equation (2) [14].

$$\sigma = \frac{l}{A}\frac{1}{R} = \frac{G}{R} \qquad (2)$$

In this equation, *l* is defined as the length of the current path (cm) and *A* is defined as the cross section of the current path (cm^2). The ratio of *l/A* is typically denoted as *G* (cm^{-1}), the cell constant, and this represents the geometry of the measurement setup. For solid materials, the dimensions of the current path typically coincide with the material's geometry and hence the cell constant is well-defined. However, the present study focusses on liquid silicate slag. Hence, the material is confined in a container and electrodes need to be submerged in the liquid to perform resistance measurements. As a result, the current between the electrodes can travel throughout the entire volume of the container and the current path is ill-defined. Therefore, a calibration is required to take into account the geometry of the current path. During this calibration, the resistance of a solution with a well-known conductivity is measured to determine the cell constant G (cm^{-1}) for the particular setup as shown in Equation (3). The calibration procedure is typically carried out at room temperature using standard aqueous KCl solutions with a well-known conductivity value [16,17].

$$G = R\sigma_{standard} \tag{3}$$

While carrying out the calibration procedure, the temperature needs to be measured to take into account the temperature dependency of the conductivity, which is generally assumed to be Arrhenian [4]. As such, Equation (4) represents the electrical conductivity as a function of temperature with σ_0 the pre-exponential factor (S/cm), E_a the activation energy (J/mol), *R* the universal gas constant (J/mol.K) and *T* the temperature (K).

$$\sigma(T) = \sigma_0 exp\left(\frac{-E_a}{RT}\right) \tag{4}$$

Moreover, since the cell constant takes into account the geometry of the measurement setup, it is evident that the immersion depth of the electrodes during calibration and high temperature experiments should be the same. Finally, it should be noted that the

calibration procedure is only accurate when the current path is invariant with respect to the investigated liquid, the electrode configuration and the electrodes [18]. These conditions allowed Schiefelbein et al.[18] to make a classification between so called low and high accuracy measurement techniques (as discussed in more detail in section 2.2).

As mentioned in the introduction, a slag is composed of metal oxides and thus it is considered an ionic liquid composed of oxygen anions and different metal cations. In the absence of multivalent ions such as Fe in the slag, the current is only carried by the metal cations in the slag. Therefore, direct current (dc) measurements are impossible since the moving ions will become stationary after a certain amount of time at the slag-electrode interface due to polarisation, which would block any current between the electrodes [19]. If multivalent ions are present, then electronic conduction due to electron hopping will still take place when applying a dc current [19]. This, however, is beyond the scope of the current study.

In this study, the focus is put on measuring the ionic (or total) conductivity of a slag, so that measurements with an alternating current (ac) should be applied. As a result, an impedance Z (Ω) is measured which is dependent on the applied frequency f (Hz) and is also composed out of a real Z_{real} (Ω) and an imaginary part Z_{imag} (Ω) as denoted in Equation (5) in which j is defined as the imaginary unit.

$$Z(f) = Z_{real}(f) + jZ_{imag}(f) \quad (5)$$

Physically, Z_{real} corresponds to electrical resistances of the sample within the measurement cell. Therefore, in order to determine the liquid's electrical conductivity, it is necessary to isolate the real impedance related to the solution resistance. In a first step, the impedance is recorded as a function of the frequency via a frequency sweep

for which the results can be visualised in a Nyquist plot as shown on the left side of Figure 1. This Nyquist plot can be divided into two regions: a high frequency region corresponding to an inductive tail and a low frequency region corresponding to a semi-arc [20–25]. The high frequency tail is the result of the solution resistance and the induction due to the long wires needed to connect the electrodes/melt with the measurement device [20,21,23], while the low frequency semi-arc is the result of the solution-electrode interface [6,24].

In a second step, the solution resistance $R_{solution}$ should be determined which can be done via several methods. A first method is to fit an equivalent circuit to the recorded impedance spectrum [20,21,23,24,26–28] similar to the circuit as visualised in Figure 1. This technique is more commonly known as Electrochemical Impedance Spectroscopy (EIS). It should be noted that the interface element here is denoted as a general impedance $Z_{interface}$. This element is typically composed of a charge transfer resistance R_{ct} in parallel with a double layer capacitance C_{dl} or a Constant Phase Element (CPE) representing the ion polarization at the interface [24,28]. Other authors have included an additional Warburg diffusion element W in series with the charge transfer resistance as they found that the ion movement was limited by diffusion at low frequencies [20,21,26,29]. A second method [6,22,28] is to determine the solution resistance at the high frequency intersection of the impedance spectrum with the $Z_{imag} = 0$ axis provided that the system is not influenced by large inductive effects.Therefore, this technique avoids the need for interpreting the impedance spectrum and selection of a correct equivalent circuit. Finally, it is also possible to carry out measurements at a single frequency f in the high frequency region corresponding to the vertical inductive tail [17,30]. This is on the condition that the real impedance $Z_{real}(f)$ at the chosen frequency f equals the value of Z_{real} at the $Z_{imag} = 0$ axis intersection though. Due to the vertical inductive tail, a region

of frequencies f that satisfy the above condition typically exists. The advantage of this technique is that impedance measurements can be carried out more quickly as the full frequency range does not need to be scanned to obtain a single value for the solution resistance. As such, the solution resistance can be continuously monitored as a function of time.

2.2. Overview measurement setups

In the previous section, it was discussed that both a container/crucible and a set of electrodes are needed to carry out electrical conductivity measurements on liquids. Hence, the combination of crucible and electrodes will be defined as the measurement cell since both influence the cell constant and consequently the measurements.

First, the different electrode configurations are discussed. The most common configurations are depicted in Figure 2. In order to perform electrical conductivity measurements on a liquid, the setup requires at least two immersed electrodes to apply a current I and measure a voltage V from which the impedance Z can be calculated. The most basic setup is thus a two-electrode setup (Figure 2 a) in which two electrodes (plates, rods or wires) are immersed into the liquid. Within this setup, the current path spreads out in all directions from both electrodes. As the current path cannot be confined, the setup does not comply with the condition of invariance of the current path with the liquid, the electrode configuration and the electrodes [14]. Due to this complex current path, the calibration procedure could introduce some error. Figure 2 b and c depict two commonly used variations of the standard two-electrode configuration which are known as the central electrode and ring electrode setup, respectively. For the central electrode technique, the crucible is made from a conductive material and functions as the second electrode. Within this setup, the current path is also complex and in addition, the large electrode area results in a small cell constant *G*. Looking at

Equation (2), this will result in a low resistance *R* for highly conductive liquids which may introduce large errors [30]. For the ring electrode setup, a clear current path is defined between the central and cylindrical electrode. Unfortunately, fringe currents above and underneath the cylinder are still present which still implies a complex current path [14]. For the previous three techniques, it should be noted that both electrodes measure the current and voltage. As depicted in the left part of Figure 3, this results in the wire resistance being included in the impedance measurements and thus a correction for the measured impedance is needed [25,26,31]. This correction is typically measured via short-circuiting the circuit via a metallic wire and is measured as a function of temperature to take into account the temperature dependency of the resistance [25,26]. Pommier et al. [25] investigated the influence of the cable impedance on the conductivity of several melts with varying conductivity. They concluded that this correction may significantly influence the conductivity of highly conductive melts, i.e. melts with a corresponding resistance equal to or lower than that of the cable corrections. On the other hand, if the melt is more resistive, the influence of the cable corrections is less pronounced. Both Pommier et al. [25] and Sun and Guo [26] report cable corrections of the order between 1-2 Ω.

In order to circumvent corrections for the wire resistance, a four-electrode configuration (Figure 2 d) can be used in which the current carrying and voltage sensing electrodes are separated. As shown in the equivalent circuit in the right part of Figure 3, this results in the wire resistance being isolated from the solution impedance. Pommier et al.[25] compared a two-electrode and four-electrode setup for a borosilicate melt and found that the correction for the wire resistance could result in large errors for highly conductive liquids at high temperatures since the solution's resistance might be of an equal or even lower order of magnitude than the wire correction resistance. On the

other hand, a four-electrode configuration is rather sensitive to the electrode geometry and placement relative to each other as the impedance is dependent on the distance between both voltage electrodes, the voltage and current electrodes and the size of the voltage electrodes. This sensitivity is caused by interference from the voltage electrodes with the electric field from the current electrodes [31]. Hence, in order to reduce measurement errors, the measured impedance can be increased via increasing the distance between the voltage electrodes, decreasing the distance between current and voltage electrodes or also by reducing the size of the voltage electrodes. Another point of attention with four-electrode configurations is that they are prone to measurement artefacts without physical meaning when performing frequency sweeps [31–33]. As a result, EIS measurements and fitting the spectrum to equivalent circuits should be done with care to prevent that these artefacts are included in the data-analysis when determining the solution resistance.

So far, the electrode configurations required a calibration procedure as the current path was not confined. These techniques typically have an accuracy around 5%-15% [13,30]. To increase the measurement accuracy, some authors have developed calibration-free techniques for liquid slags [6,14]. The setup from Schiefelbein et al.[14] consists of a coaxial cylinder technique similar to the ring electrode setup. Therefore, at a single immersion depth, the configuration also suffers from fringe currents, but their contribution can be isolated when measuring at multiple immersion depths. They validated their setup with standard conductivity KCl solutions and found that their results deviated only 0.5% from the theoretical conductivity. Unfortunately, it was found that this technique is inadequate to accurately carry out conductivity measurements if the liquid's conductivity is higher than 0.1 S/cm [34]. As a result, its applicability for high conductivity slags is limited. The second technique of Zhang et al.[6] is capable of

blocking uncontrolled spreading of the current via adding non-conductive parts to the crucible cell. This is for example done by placing two Pt-electrodes at the outer sides of a non-conductive boronnitride (BN) crucible or via placing an alumina plate at the bottom of a molybdenum (Mo) cylindrical crucible. In both setups, the cell constant has to be defined post mortem via measuring the cross section of the quenched sample, meaning that the sample needs to be extracted in one piece from the setup. They also verified their Mo crucible setup with standard KCl solutions at room temperature and found a deviation of 2.4% to the theoretical value. For high temperature measurements, they reported a standard deviation of 2.6% and 7.4% for the Mo and BN crucible setup, respectively. The authors attributed the difference in error of the setups due the sample's irregular shape/cross section within the BN crucible, which introduced difficulties in determining the cell constant.

The final contribution to the measurement cell is the crucible material which can have an important impact. Typically, a choice is made between metallic or oxidic crucibles. Metallic crucibles have the advantage that they can be made from inert materials with respect to the slag such as platina or gold. However these crucibles are conductive and thus some current can pass through the crucible walls which influences the measurements [16,28]. On the other hand, oxidic crucibles are non-conductive, but they do dissolve in the slag which alters the chemical composition of the sample, and thus its electrical conductivity over time. To take this variation into account, it is advised to compare the slag's composition before and after the experiment [30]. As a way to decrease the crucible's interference, the ideal choice would be to have a slow/non-dissolving oxidic crucible for a certain slag system. This ideal situation is unfortunately seldom an option.

2.3. Measurement procedures and setups in PbO slag systems

As already mentioned, the second goal of this paper was to investigate a measurement procedure for carrying out electrical conductivity experiments in PbO containing slags. Therefore, an overview is also provided of the methodologies and measurement setups used for these specific systems in literature. As mentioned in our previous study [15], the binary SiO_2-PbO system has already been studied by multiple authors [35–41] which makes it an ideal system to verify our methodology. In addition, there also exist some other studies which investigate ternary PbO containing systems as well [38,42,43]. The electrical conduction mechanism of a binary SiO_2-PbO system was investigated by both Bockris et al. [36] and Ito et al. [37] using current efficiency methods via electrolysis of the PbO-SiO_2 using an inert Pt anode and lead cathode. Both authors found a current efficiency of nearly 100%, which indicates that all electrons from the lead cathode are used to reduce the lead cations to metallic lead. As such, no electronic conduction takes place in this system as this would imply efficiencies below 100%. Hence, only ionic conduction is present. As a result, AC impedance measurements are sufficient for investigating these slag systems. Moreover, Bockris et al. [36,44] determined that in liquid silicate slags, ionic conduction occurs via the movement of metal cations, except the silicon cation Si^{4+} as this cation forms a strong bond with oxygen anions, which results in the formation of a polymeric network of SiO_4^{4-} tetrahedra. On the other hand, Pb^{2+} has a much weaker bond with the oxygen anions and thus it is able to move throughout the silicate network which allows the slag to be conductive.

As for the measurement techniques, the majority of the above listed authors [36,40,41] measure the conductivity via a two-electrode conductivity setup using both Pt wires and a Pt crucible at a single frequency between 1 – 10 kHz. Ejima et al. [39], Ito et al.[37] and Kawahara et al.[42] used a ring-electrode setup instead, while Schellinger et al.[35]

and Uday et al.[43] used a silica and alumina crucible, respectively. The only exception for the single frequency measurement is the study carried out by Ashizuka et al.[40], who measured the impedance between 1 and 10 kHz and found a frequency dependency of the impedance in this region. To determine the solution resistance, they extrapolated the impedance to an infinite frequency. This could, however, indicate that they did not carry out measurements in a frequency range corresponding to the inductive tail as explained earlier in section 2.1(Figure 1).

Typical temperature ranges for conductivity experiments with PbO systems lie between 750 °C and 1250 °C. Bockris et al.[36] mentioned that PbO could evaporate at elevated temperatures. However, it is unclear whether they systematically investigated the slag composition after each experiment. Likewise, Saito et al.[41] mentions that the slag composition before and after each experiment was found to be similar, but nor slag compositions, nor an experimental technique used to investigate this are provided. The studies carried out in an oxidic crucible [35,43] also did not report any post-experiment chemical compositions either. To conclude, it was found that all previous electrical conductivity data were obtained from experimental setups for which a cable correction is required, inert crucibles seem to be the preferred choice for these experiments and that PbO evaporation is only scarcely mentioned. These findings and drawbacks of earlier studies were taken into account when developing a methodology for the experiments in the current study.

3. Materials & methods

3.1. Preparation of slag samples and characterization

In this study, a single binary SiO_2-PbO system with a weight ratio of 75/25 PbO/SiO_2 will be measured. The slag sample was prepared form high purity (> 99.9%) powder

chemicals (SiO_2, PbO) provided from Sigma Aldrich. The powders were first mixed and this mixture was then melted in a high-frequency induction furnace (Hüttinger TIG 20/ 100) in an Al_2O_3 crucible. The melting temperature was set to 950 °C to reduce the slag viscosity and thus to ensure a sufficiently quick homogenisation. At this temperature, the slag was fully liquid and air was continuously blown (24 l /h) through the slag bath to ensure a further mixing of the chemicals. As Al_2O_3 dissolves in the slag at this temperature, the holding time was limited to 30 – 40 minutes to minimize this dissolution. Finally, the slag was quenched via pouring the hot melt in water. Several quenched pieces were then cold embedded using Epofix resin and were ground and polished up to a 1 µm abrasive particle size. These pieces were investigated via a scanning electron microscope (SEM, JEOL, JSM-7600, FEG-SEM) which is equipped with an energy-dispersive X-ray spectroscopy detector (EDS, Oxford Instruments, x - Maxn Silicon Drift Detector). As such, both the chemical composition of the slag, including the Al_2O_3 content from the smelting procedure, as well as the presence of solids could be analysed simultaneously. The used acceleration voltage during these measurements was 15 kV. To prevent charges building up on the sample, it was first carbon coated using physical vapor deposition.

3.2. Measurement setup

A schematic representation of the electrical conductivity measurement setup is given in Figure 4. The setup is constructed around a vertically mounted HTRV 1800/100/500 Carbolite resistance tube furnace with a tube length of 755 mm. The temperature is controlled via a programmable temperature controller (Eurotherm) such that the thermocouple next to the crucible was kept at the desired temperature. For the conductivity measurements, a four-electrode conductivity setup is chosen as it circumvents the need for cable corrections and potential errors for high conductivity

liquids which are associated with two electrode configurations. In addition, this setup eliminates the need for complex configurations and extensive measurement procedures related with the calibration free methods. The electrodes are made of 800 mm long and 1 mm thick Pt-10%Ir wires which are inserted into an Al_2O_3 tube with an outer diameter of 1.2 mm. It was found that a small gap between the electrodes and twin tube holes is sufficient to keep the wires at their position during measurements. Additionally, it provides a tolerance to still move the wires deeper into the tubes if the tips need to be replaced as a result of excessive bending or damage. Each electrode is inserted into a separate tube to avoid the appearance of the artefact that during the initial frequency sweep negative real impedances during the calibration [33].

A schematic representation of the wire geometry is also provided in Figure 4. In this figure, d_0 is defined as the distance between the centre of the inner and outer electrode and was measured to be around 6 mm, while d_i is the distance between the inner electrodes which was equal to 10.5 mm. This geometry allowed to increase the cell constant G of the measurement cell. The immersion depth h_{imm} and slag bath height h_{bath} remained the same, being respectively 3 mm and 10 mm. The electrodes are connected via extension wires to a Gamry Interface 1010E potentiostat which measures the slag's impedance. The immersion depth (h) of the electrodes in the slag bath is controlled via an EAS4X linear unit provided by Oriental Motor with a minimal step size of 0.01 mm which is placed on the top of the furnace. Conductivity experiments were carried out with a crucible made from a thin walled Pt-10%Ir alloy with an outer diameter of 42 mm and a height of 33 mm. A metallic crucible was chosen due to its inertness with respect to the investigated slag samples. As a comparison, a conductivity experiment at high temperature was also carried out in an oxidic Al_2O_3

crucible with an inner diameter of 36 mm and a height of 33 mm to investigate the effect of a non-inert crucible on the measurements.

The crucible itself is positioned in the centre of the furnace on a ceramic insulation plug. This ceramic plug is placed on a platform which is connected to another linear unit (EAS6X Oriental motor) at the bottom of the furnace. Using this linear unit, it is possible to evacuate the crucible from the furnace within 5 seconds. Thus, the material can be poured from the crucible in water making quenching possible for the present experiments. Finally, a type R thermocouple is inserted from the top of the furnace which is placed next to the crucible containing the liquid slag. The furnace's heating elements are adjusted based on the readings of this thermocouple, which ensures an accurate temperature control of the crucible and the liquid slag.

3.3. Cell calibration

The cell constant of the setup was determined via calibration with aqueous 1 D and 0.1 D (Demal[1]) KCl solutions at room temperature. The crucible was filled up to a height of 10 mm as this corresponds with the desired slag bath volume for high temperature experiments. During calibration, the temperature was recorded to take into account the temperature dependency of the conductivity. For the aqueous low temperature measurements, the impedance was measured galvanostatically with an excitation current of 100 µA. First, the bath surface was located via slowly descending the electrodes while measuring the impedance. The bath surface could be located due to a sudden drop in the impedance and less fluctuating values as opposed to readings in air. The electrodes were then lowered in the bath to the desired immersion depth of 3 mm.

[1] The demal (D) reflects 1 g of solute per dm^3 at 0 °C.

Second, a frequency sweep was carried out between 500 kHz and 0.1 Hz. From this sweep, it was found that the real impedance was (nearly) constant between 10 and 100 kHz and equal to $Z_{real}(f^*)$ for which $Z_{imag}(f^*)$ = 0. For the 1 D KCl solution, the impedance was recorded for 25, 50 and 75 kHz, while for 0.1 D KCl, it was recorded at 10, 50 and 100 kHz. This difference in frequencies is chosen due to a slight gradient between 10 and 100 kHz still being present within the 0.1 D KCl measurement. The impedance at each frequency was measured continuously for ten minutes to determine the solution resistance R_{sol}. In addition, the solution resistance was also calculated via fitting the frequency sweep data to an equivalent circuit. Similar to our previous work[15], the calibration procedure was carried out before each high temperature measurement.

3.4. High temperature electrical conductivity measurements

As for the high temperature experiments, first the mass needed to have a slag bath of 10 mm was determined. This was done via the slag's density, for which the data was obtained from Cnockaert et al. [45]. The temperature profile of the experiments performed in inert metallic crucibles is depicted in Figure 5. The sample was first brought to 1100 °C via a heating rate of 5 °C/min. It was then initially kept at this temperature for 30 minutes to ensure that the slag is fully liquid. It was decided to choose 1100 °C as the first temperature instead of 1000 °C to ensure a faster melting of the solid slag and to dissolve any solids that could have precipitated during heating up of the slag. After this initial thermal equilibration, the slag surface was determined similar to the procedure at low temperature and the electrodes were also lowered to an immersion depth of 3 mm. Impedance measurements were also carried out galvanostatically with a 100 µA excitation current. First, a frequency sweep (between 100 kHz and 0.1 Hz) was carried out which was followed by a single frequency measurement. The frequency sweep showed that the real impedance was constant

between 1 and 10 kHz, which is in agreement with the frequency range studied by other authors [35,36,38,41]. Therefore, single frequency measurements were carried out at 5 and 10 kHz to determine R_{slag}. Similar to the measurements at low temperature, the slag's resistance was also determined from the frequency sweep by fitting the impedance with an equivalent circuit. This provides an internal check for the present experiments whether the conductivity values from both methods agree with each other.

After a single impedance measurement, a similar heating/cooling ramp of 5 °C/min was used to go to the next temperature, where the same measurement procedure was repeated except for the determination of the slag bath. The holding time at subsequent temperatures was reduced to 20 minutes as thermal equilibrium was reached sooner. The conductivity was measured both at the beginning and the end at 1100 °C as this allows us to quantify any change in the electrical conductivity due to PbO vaporisation. After the final measurement, the electrodes were lifted above the slag bath and the crucible was evacuated from the furnace via the bottom linear unit as depicted in Figure 4. The Pt-Ir crucible was then poured into water and the slag's chemical composition was analysed via SEM-EDX. The electrodes and crucible were then cleaned in a 37% HCl solution at 80 °C to remove any remaining slag. It should be noted that in most cases, the remaining solidified slag had to be mechanically removed from the electrodes as well. Each composition was measured three times via the same procedure to make an estimation of the standard deviation and the accuracy of our measurement setup. For the measurement in the oxidic Al_2O_3 crucible, the frequency sweep and single frequency measurement were only carried out at 1100 °C. To investigate the crucible dissolution, the impedance was continuously measured at 5 kHz for one hour. After this measurement, the crucible was also evacuated from the furnace similar to the metallic ones, but the crucible was cooled down in air to preserve

the integrity of the crucible which allowed to investigate the Al_2O_3 dissolution as a function of the distance to the crucible wall via SEM-EDX.

4. Results & Discussion

4.1. Calibration

The average cell constant and standard deviation obtained via the calibration procedure with 1 D and 0.1 D KCl solutions for the metallic Pt-Ir and oxidic Al_2O_3 crucible are plotted in Figure 6 a). For 1 D KCl and 0.1 D KCl, a cell constant and standard deviation of 0.23 cm^{-1} (± 5.11%) and 0.22 cm^{-1} (± 6.38%) was found for the metallic crucible, respectively. On the other hand, the cell constant for the oxidic crucible was significantly higher: 0.59 cm^{-1} and 0.60 cm^{-1} for the different solutions, respectively. These data thus illustrate that the current path within the four-electrode conductivity setup is dependent on the measurement cell and solution as mentioned in section 2. Between the different crucible materials, a difference in cell constant of almost a factor 3 was found, which indicates that some portion of the current indeed passes through the more conductive metallic crucible. In addition, a small difference between both calibration solutions was found during each measurement but this was typically limited to about 3%. This shows that the current path is relatively independent of the conductivity of the measured solution. In addition, as signified by the standard deviation, there also exists some difference in the cell constant after cleaning of the electrodes and reassembling the setup. As discussed in our previous research [15], such differences were observed as well after disassembly of the setup for cleaning. During cleaning, it was sometimes necessary to break of solidified slag pieces using a plier, some bending of the electrodes or damage to the electrode surface could be made, which in turn could introduce these errors.

Another point of interest is a decrease in cell constant of about 0.3 cm^{-1} when comparing the current setup with our earlier setup with two electrodes in the same Al_2O_3 tube and with smaller gold crucibles. For the present setup, the distance between the inner electrodes d_i was increased from 5 mm to 9.5 mm, and the distance between the crucible wall and the outer electrodes was increased from 5.5/7.5 mm to 9.25 mm. These adaptations should lead to a larger measured impedance since the length of the current path between the voltage sensing electrodes is increased, while less current should be able reach the conductive Pt-Ir crucible. However, the distance between the inner and outer electrodes d_o was increased as well from 1 mm to 5 mm as the electrodes were put in separate Al_2O_3 tubes to prevent measurement artefacts related to the negative real impedances. As mentioned in section 2, increasing the distance d_o between current carrying and voltage sensing electrodes will lead to lower impedances. It thus seems that the change in d_0 between our setups was dominant for the resulting cell constant. Overall, our results confirm that a four-electrode conductivity setup is highly sensitive to the cell geometry and crucible materials.

Figure 6 b) and c) show the Nyquist plot of the frequency sweep within the 1 D KCl and 0.1 D KCl solutions for the metallic crucible as well as the equivalent circuit used to fit both impedance spectra. It was found that the inductance of the wires at high frequency was still measured for the 1 D KCl solution, while this was not the case for the 0.1 D KCl solution. This could potentially be related to the higher measured impedances for the 0.1 D solution which may be dominant over the high frequency artefact related to the wire inductance. At lower frequencies, the Nyquist plot shows a semi-arc which was fitted to a resistance R_{ct} and a constant phase element (CPE) Q_{dl} in parallel with each other. For the 1 D KCl solution, an inductive artefact was found for frequencies below 30 Hz and thus these data points were not used for determining the equivalent

circuit. Lvovic and Smiechowski[31] measured a similar artefact and attributed this to a parasitic current from the voltage electrodes. As a result, both spectra were fitted to a (modified) Randles circuit similar to the studies of Simmonet et al.[28] and Pommier et al.[25]. The solution resistance R_{sol} obtained from the equivalent circuit was then used to calculate the cell constant via Equation (3). The cell constant from the single frequency measurement $G_{singfreq}$ and from the equivalent circuit fit $G_{circuit}$ are compared with each other in Figure 6 d) for both calibration solutions. It was found that both cell constants do not differ more than 1% from each other and thus it is concluded that both methods are indeed equivalent.

4.2. High temperature results

The chemical composition of the slag obtained from the melting procedure is provided in Table 1. As shown, the slag seems to have some excess in PbO in comparison to the desired value of 75 wt%. In addition, a slight amount of Al_2O_3 was measured as well which was expected due to dissolution of the Al_2O_3 crucible. It should be noted though that this value is rather small with a significant standard deviation compared to the measured value. As such, the Al_2O_3 content should only be considered as an indication that some crucible dissolution happened during the slag preparation step. Also, no solid particles were found within the sample via SEM.

*Table 1. Chemical composition (in wt%) and associated standard deviation for each composition of the investigated slag. *$T_{liquidus}$ was calculated via Factsage 8.1, FTOxid* [46]

Wt%	PbO	SiO_2	Al_2O_3	$T_{liquidus}$ (°C)*
75/25 slag	76.92 ± 0.11	22.65 ± 0.11	0.43 ± 0.09	751 °C

Figure 7 shows the natural logarithm of the conductivity as a function of the inverse of the temperature, for both the Pt-Ir and Al_2O_3 crucible as well as the standard deviation. The standard deviation on the absolute values for the different temperature measurements was found to be within the range of 6.96% and 10.07% which is somewhat higher than the values determined from the low temperature calibration. As the measured impedance during high temperature measurements was within the range of 5 Ω to 0.6 Ω, it is expected that relatively small changes in the measured impedance could already result in relatively large errors when expressed in percentage. However, it is unclear how the standard deviations and/or experimental in literature were determined, i.e. on the absolute or logarithmic values. Hence, the standard deviations on the logarithmic values are also reported. These were found to be in the range of 3.18% and 7.16% which do better agree within the expected experimental error range. Furthermore, the small impedance values also justifies the need for a four-electrode measurement setup to circumvent any potential error during the cell correction. For the current setup, the correction due to cable impedances was estimated via measuring the resistance of the wires connecting the potentiostat with the electrodes and calculating the resistance of the electrodes in the furnace. To take into account the temperature dependency of the electrodes' resistance, the temperature profile of the oven was simplified to a linear one with one end of the electrode at the slag's temperature, while the other was at room temperature. Via this approach, the total electrode's resistance could be found via integration over the length of the electrodes. Using this approach, a value between 0.78 and 0.88 Ω is found, which is of a similar magnitude as reported in literature [25,26]. As the cable correction is of a similar magnitude as the actual resistance of the melt, any error or uncertainty in this correction procedure may affect the conductivity significantly.

Figure 7 also shows that our data shows a good fit with an Arrhenian temperature dependency, which is expected since the electrical conductivity was measured above the slag's liquidus temperature [6]. The Arrhenian activation energy E_a was found to be equal to 103.51 ± 1.03 kJ/mol.K. Given the low standard deviation on the activation energy, it is shown that our setup generates reproducible data in terms of the slag's temperature dependency. Finally, the data point of the conductivity measurement in the Al_2O_3 crucible at 1100 °C was found to agree with the measurement in the Pt-Ir crucible. This illustrates that our calibration procedure is independent of the chosen crucible material and thus that the cell constant is able to compensate for different current paths due to the crucible material.

Figure 7 b) and c) compares the data of the current study with those from several authors as a function of the PbO content at 1000 °C and 1100 °C. From these graphs, it is clear that our data points are somewhat below the expected values obtained by Ito et al.[37] and Ejima et al.[39] who investigated similar compositions. One possible explanation for this deviation could be that our slag contained a certain amount of alumina as detected from the EDX-measurement. Suginohara et al.[38] found that the electrical conductivity of PbO-SiO_2 decreases significantly when adding minor amounts of Al_2O_3. They measured a decrease of 24% for the electrical conductivity when adding 1.82 wt% of Al_2O_3 to a 82/18 PbO/SiO_2 binary slag. This drastic drop of the electrical conductivity could be attributed to the amphoteric character of Al_2O_3 as the Al^{3+} cations may be incorporated into the silica network via charge compensation by the present Pb^{2+} cations, leaving less network modifying Pb^{2+} cations available for conducting the current [4]. Another explanation could be related to the used measurement setup from both authors as they used a ring-electrode setup, which requires a correction for the wire resistance, which increases as a function of temperature. Ito et al.[37] mentioned

within their work that this correction for the electrodes was rather high, but did not provide any numerical value for this correction. Adapting Equation (2) to also include the wire resistance, one sees that if both R_{slag} and R_{wires} are low and of a similar order of magnitude, it is possible to overestimate the slag's electrical conductivity due to measurement inaccuracies.

$$\sigma_{slag} = \frac{G}{R_{measured} - R_{wires}} \quad (6)$$

Considering the data of Ejima et al.[39], this might provide an explanation for the divergence of their electrical conductivity data from those of other authors at higher PbO contents. The data from Ito et al.(Ito 1960) on the other hand does agree with other studies at higher PbO contents though. Unfortunately, it is not uncommon for electrical conductivity data to give significantly different values between different studies on similar slag compositions [13]. Therefore, obtaining an experimental data point with a similar order of magnitude is already considered a good result. Moreover, the obtained activation energy was compared in Figure 7 d) and shows that the obtained activation energy follows the expected trend as a function of the PbO content and lies within the range of other studies. Therefore, it is concluded that our experimental setup and methodology are capable of providing similar results as the setups used in literature for the investigated system.

The impedance spectrum obtained via the frequency sweeps was investigated via Nyquist plots as well, which are provided in Figure 7 e). These plots also have the typical shape of a high frequency inductive tail in combination with a low frequency curvature which resembles a Randles circuit. Similar to the Nyquist plot for the 1D KCl solution, these spectra were also fitted with a modified Randles circuit as shown in Figure 6 b). As opposed to the low temperature measurements, no measurement

artefacts from the four-electrode setup were present. This may perhaps be related to the solution type, as a slag is a full ionic liquid whereas the KCl solution is an aqueous solution containing solvated ions. This would thus illustrate the current path's dependence on the solution type as well. Finally, the electrical conductivity was calculated via Equation (2) using the fitted values R_{slag} of the equivalent circuit and these values are compared with those from the single frequency method in Figure 7 f). As shown, the conductivity values from both methods agree well with each other, which also proves the equivalency of both methods at high temperature which was also verified by Hundermark [30].

4.3. Stability of the measurements

As mentioned in section 3.1, measurements were both carried out in a metallic Pt-Ir and in an oxidic Al_2O_3 crucible to investigate the effect of a non-inert crucible on the conductivity measurements as a function of time. In addition, it was also noted that PbO is a volatile component and thus its evaporation from the melt may also influence the measurement. This contribution was quantified in an inert Pt-Ir crucible as PbO evaporation is the only reason for a change in the chemical composition of the slag during this experiment. Comparison of the conductivity as a function of the measurement time/change in chemical composition due to PbO loss/Al_2O_3 enrichment should indicate which contribution is dominant in terms of measurement inaccuracies.

Figure 8 a) shows the conductivity as a function of the measurement time during the measurement at 1100 °C in an Al_2O_3 crucible. As can be seen, a clear continuous decrease in the electrical conductivity is observed which is attributed to the continuous increase of the Al_2O_3 content of the slag as shown in Figure 8 b). This figure shows the slag's Al_2O_3 content as a function of the distance from the crucible wall (logarithmic scales) at an immersion depth of 3 mm from the sample surface, i.e. the immersion

depth of the electrodes in the slag. In addition, the initial Al_2O_3 content of the slag is plotted as well. From the obtained compositions, it is clear that Al_2O_3 dissolution takes place as the final Al_2O_3 content in the bulk (data points at 4, 10 and 18 mm) is higher than in the sample before the conductivity experiment and that these values are outside the uncertainty range of the original measurement. It should be noted that although the absolute increase in Al_2O_3 content is rather limited, the implications on the conductivity are non-negligible. Due to the limited amount of Al_2O_3 dissolution, it is considered unlikely that the geometry of the crucible and thus the cell constant has changed considerably over the course of the experiment. However, as mentioned earlier, a similar decrease in conductivity due to small Al_2O_3 additions was observed by Suginohara et al. [38] which can be linked to the low Al_2O_3 diffusivity as indicated by the dissolution profile in Figure 8 b). As mentioned in Section 2.3, ionic conduction in slags occurs via the movement of metal cations throughout the silicate network. Thus, the contribution of a metal cation to the overall ionic conductivity, σ_i (S/cm), is dependent on the diffusivity of that cation within the melt, D_i (m^2/s), and the relation between both is expressed via the Nernst-Einstein equation [13]. In this equation z_i (-) is the charge number of the cation, F (C/mol) is Faraday's constant, c_i (mol/m^3) is the cation's concentration in the melt, R (J/mol.K) is the universal gas constant and T (K) is the absolute temperature.

$$\sigma_{slag} = \sum_i \sigma_i = \sum_i \frac{{z_i}^2 F^2 c_i}{RT} D_i \qquad (7)$$

From literature [47], it was found that the self-diffusion coefficient of Pb^{2+} at 850 °C and Al^{3+} at 1473 °C have a similar order of magnitude of 10^{-9} – 10^{-11} m^2/s. However, similar as the electrical conductivity, the diffusion coefficient has an Arrhenian temperature dependency as shown earlier in Equation (4) and thus it follows that $D_{Pb2+} > D_{Al3+}$ for

similar temperatures. As a result, during the experiment with the Al_2O_3 crucible, the slag is gradually enriched with slow moving Al^{3+} cations which will lower the overall electrical conductivity of the melt. However, as the current travels throughout the entire volume within the crucible, some current lines will pass through areas with a higher resistance to current transport due a locally increased Al_2O_3 content, for example near the crucible walls. As electrical conductivity measurements can only measure the conductivity of the entire melt, the relative contribution of these higher resistive zones to the overall electrical conductivity cannot be isolated. Due to this inhomogeneous composition profile, it is impossible to attribute a specific electrical conductivity to a certain slag composition. Besides the homogeneity issues, the slag composition also continuously changes as a function of time meaning further complications for attributing conductivity values to slag compositions. Therefore, it was concluded that Al_2O_3 crucibles are unsuitable for performing electrical conductivity measurements for binary SiO_2-PbO systems and no further experiments were carried out with this crucible.

Table 2 provides an overview of the decrease in percentage in the electrical conductivity as well as the PbO and Al_2O_3 compositions as a function of the total measurement time starting from the first single frequency measurement at 1100 °C. For the measurement with the Al_2O_3 crucible, a difference of -3.83% was found during the one hour measurement which is mainly attributed to an increase in Al_2O_3 content. Although a slight difference in PbO content was measured as well, it was found that the difference was rather small. For the measurement in the metallic crucible, the decrease in electrical conductivity is defined as follows

$$\Delta\sigma = \frac{\sigma_{1100\,°C,final} - \sigma_{1100\,°C,init}}{\sigma_{1100\,°C,init}} \quad (8)$$

From

Table 2, it thus becomes clear that the difference in electrical conductivity as a result of PbO volatilization is questionable given the large standard deviation on the PbO content value. A significant decrease in the electrical conductivity was only observed during one experiment, while for the other two, the difference was negligible. A similar result was found for the PbO concentration for which the difference is also rather limited and for which a large standard deviation is found as well. As such, PbO volatilization might not be an issue for the present slag system.

Table 2. Overview of the difference in electrical conductivity as a function of the measurement time and crucible material. In addition, the absolute change in the chemical composition of PbO and Al_2O_3 for the different measurements is provided as well.

Crucible Material	Measurement time	$\Delta\sigma$ (%)	ΔPbO $(wt\%)$	$\Delta Al_2O_3 (wt\%)$
Al_2O_3	1h	-3.83%	-0.31	+0.36
Pt-Ir	5h 20 min	-3.80	-1.67	/
Pt-Ir	5h 20 min	0.07	0.01	/
Pt-Ir	5h 20 min	0.93	0.30	/

Conclusion

The electrical conductivity of metallurgical slags has a major impact on the operation of SAF's which are typically utilized for slag cleaning operations to reduce metal losses within metal production/recycling processes. As such, obtaining reliable electrical

conductivity data is important regarding the understanding, dimensioning and operation of these furnaces. However, no standardized method for electrical conductivity methods is available and thus a variety of different methods and setups are used. The present study aimed to provide an overview of the advantages and disadvantages of each method and setup as well as selecting a suitable measurement setup.

For the present experiments, a four-electrode configuration was constructed as it provides a fast way for data collection compared to calibration-free methods, while it avoids the need for cable corrections as opposed to two-electrode setups. In addition, the study focused on the use of inert versus non-inert crucible materials for conductivity measurements via comparing a Pt-Ir with an Al_2O_3 crucible.

Experiments at room temperature with aqueous KCl solutions indicated that the cell constant is mainly influenced by both the crucible material and the relative distance of the electrodes, while the influence of the solution's conductivity was limited.

For the high temperature experiments with a binary SiO_2-PbO slag, it was found that the electrical conductivity values measured in a Pt-Ir crucible and Al_2O_3 crucible were of equal magnitude, which shows that our obtained conductivity values are independent of the resulting current path as a function of the crucible material. In addition, our results were compared to experimental literature data and it was found that both our conductivity data and Arrhenian activation energy are of similar order of magnitude. Furthermore, repetition experiments in the Pt-Ir crucible indicated that our reproducibility is slightly better than the typical range mentioned in literature for the electrical conductivity (in S/cm). On the other hand, the measured temperature dependency was very consistent between different measurements with a standard deviation less than 1%.

Finally, the effect of PbO volatilization and Al_2O_3 dissolution on the electrical conductivity was quantified. It was found that PbO volatilization had no significant effect on the electrical conductivity which was complemented via EDX as no significant PbO loss was observed as well. On the other hand, Al_2O_3 had a significant effect on the measurement as a decrease of 3.83% was observed when continuously measuring for one hour at 1100 °C. From the above results, it is concluded that reliable data can be obtained with our current setup and methodology for more complex lead-silicate slag compositions using inert crucibles.

Acknowledgements

P. Boeykens holds a grant [HBC.2020.2248] which is supported by VLAIO, the Flanders Innovation & Entrepreneurship Agency, in co-operation with Umicore. I. Bellemans holds a grant from the Research Foundation Flanders [101096/12Z7720N]. The authors would like to thank O. Vergote for his support during the high temperature experiments, E. De Ketelaere for his input on the impedance spectra and I. De Baere and P. Baele for helping with the construction of the setup.

References

1. Spooren, J. *et al.* Near-zero-waste processing of low-grade, complex primary ores and secondary raw materials in Europe: technology development trends. *Resour. Conserv. Recycl.* **160**, 104919 (2020).
2. Watari, T., Nansai, K. & Nakajima, K. Major metals demand, supply, and environmental impacts to 2100: A critical review. *Resour. Conserv. Recycl.* **164**, 105107 (2021).

3. Norgate, T. & Jahanshahi, S. Low grade ores – Smelt, leach or concentrate? *Miner. Eng.* **23**, 65–73 (2010).

4. Mills, K. C. The Estimation Of Slag Properties. *South. African Pyrometallurgy 2011 Int. Conf.* 1–52 (2011).

5. Tian, H. *et al.* Comprehensive review on metallurgical recycling and cleaning of copper slag. *Resour. Conserv. Recycl.* **168**, 105366 (2021).

6. Zhang, L., Malfliet, A., Blanpain, B. & Guo, M. In Situ Electrical Conductivity Measurement by Using Confocal Scanning Laser Microscopy. *Metall. Mater. Trans. B 2021 524* **52**, 2563–2572 (2021).

7. Bellemans, I., De Wilde, E., Moelans, N. & Verbeken, K. Metal losses in pyrometallurgical operations - A review. *Adv. Colloid Interface Sci.* **255**, 47–63 (2018).

8. De Wilde, E. *et al.* Origin and sedimentation of Cu-droplets sticking to spinel solids in pyrometallurgical slags. *Mater. Sci. Technol. (United Kingdom)* **32**, 1911–1924 (2016).

9. Friedrich, B. *et al.* The Submerged Arc Furnace (SAF): State-of-the-Art Metal Recovery from Nonferrous Slags. *J. Sustain. Metall.* **4**, 77–94 (2018).

10. Grzella, J. *et al.* Metallurgical Furnaces. in *Ullmann's Encyclopedia of Industrial Chemistry* (2003). doi:doi:10.1002/14356007.b04_339.

11. Eric, R. H. Slag properties and design issues pertinent to matte smelting electric furnaces. *J. South African Inst. Min. Metall.* **104**, 499–510 (2004).

12. Karalis, K. T. *et al.* A CFD analysis of slag properties, electrode shape and immersion depth effects on electric submerged arc furnace heating in ferronickel processing. *Appl. Math. Model.* **40**, 9052–9066 (2016).

13. Thibodeau, E. & Jung, I. H. A Structural Electrical Conductivity Model for Oxide Melts. *Metall. Mater. Trans. B Process Metall. Mater. Process. Sci.* **47**, 355–383 (2016).

14. Schiefelbein, S. L. & Sadoway, D. R. A High-Accuracy, Calibration-Free Technique for Measuring the Electrical Conductivity of Molten Oxides. *Metall. Mater. Trans. B Process Metall. Mater. Process. Sci.* **28**, 1141–1149 (1997).

15. Boeykens, P., Bellemans, I., Verbeken, K., Scheunis, L. & Van den Bulck, A. Methodological investigation of a four-electrode electrical conductivity set-up in a binary SiO2 -PbO system. in *Copper 2022* 307–318 (2022).

16. Gruener, G., Dembinski, K., Bouvier, A., Loup, J. P. & Odier, P. Measurements of conductivity in liquids. Application to 2CaOAl2O3SiO2. *EPJ Appl. Phys.* **4**, 101–106 (1998).

17. Barati, M. & Coley, K. S. *Electrical and electronic conductivity of CaO-SiO2-FeO x slags at various oxygen potentials: Part I. Experimental results*. *Metallurgical and Materials Transactions B: Process Metallurgy and Materials Processing Science* vol. 37 (2006).

18. Schiefelbein, S. L., Fried, N. A., Rhoads, K. G. & Sadoway, D. R. A high-accuracy, calibration-free technique for measuring the electrical conductivity of liquids. *Rev. Sci. Instrum.* **69**, 3308–3313 (1998).

19. Fried, N. A., Rhoads, K. G. & Sadoway, D. R. Transference number measurements of TiO2-BaO melts by stepped-potential chronoamperometry. *Electrochim. Acta* **46**, 3351–3358 (2001).

20. Martin-Treceno, S., Allanore, A., Bishop, C. M., Watson, M. J. & Marshall, A. T. Determination of the Partial Contributions to the Electrical Conductivity of TiO2-SiO2-Al2O3-MgO-CaO Slags: Role of the Experimental Processing Conditions. *Metall. Mater. Trans. B Process Metall. Mater. Process. Sci.* **53**, 798–806 (2022).

21. Caldwell, A. H., Lai, E., Gmitter, A. J. & Allanore, A. Influence of mass transfer and electrolyte composition on anodic oxygen evolution in molten oxides. *Electrochim.*

Acta **219**, 178–186 (2016).

22. Laumonier, M., Gaillard, F. & Sifre, D. The effect of pressure and water concentration on the electrical conductivity of dacitic melts: Implication for magnetotelluric imaging in subduction areas. *Chem. Geol.* **418**, 66–76 (2015).
23. Judge, W. D., Paeng, J. & Azimi, G. Electrochemical characteristics of molten iron electrodes in slag and electrochemical properties of their interface. *Electrochim. Acta* **389**, 138755 (2021).
24. Pommier, A., Leinenweber, K. & Tasaka, M. Experimental investigation of the electrical behavior of olivine during partial melting under pressure and application to the lunar mantle. *Earth Planet. Sci. Lett.* **425**, 242–255 (2015).
25. Pommier, A., GAillArd, F., Malki, M. & PichAvAnt, M. Methodological re-evaluation of the electrical conductivity of silicate melts. *Am. Mineral.* **95**, 284–291 (2010).
26. Sun, C. Y. & Guo, X. M. Electrical conductivity of MO(MO=FeO, NiO)-containing CaO-MgO-SiO 2-Al2O3 slag with low basicity. *Trans. Nonferrous Met. Soc. China (English Ed.* **21**, 1648–1654 (2011).
27. Harada, Y., Saito, N. & Nakashima, K. Impedance measurement and equivalent circuit analysis of binary alkali silicate melts. *ISIJ Int.* **59**, 421–426 (2019).
28. Simonnet, C., Phalippou, J., Malki, M. & Grandjean, A. Electrical conductivity measurements of oxides from molten state to glassy state. *Rev. Sci. Instrum.* **74**, 2805–2810 (2003).
29. Harada, Y., Sukenaga, S., Saito, N. & Nakashima, K. Structural Analysis of Mixed Alkali Silicate Melts through 29Si MAS-NMR and Impedance Measurements. *ISIJ Int.* **59**, 1956–1965 (2019).
30. Hundermark, R. The electrical conductivity of melter type slags. (2003).

31. Lvovich, V. F. & Smiechowski, M. F. AC impedance investigation of conductivity of automotive lubricants using two- and four-electrode electrochemical cells. *J. Appl. Electrochem.* **39**, 2439 (2009).

32. Fafilek, G. The use of voltage probes in impedance spectroscopy. *Solid State Ionics* **176**, 2023–2029 (2005).

33. Veal, B. W., Baldo, P. M., Paulikas, A. P. & Eastman, J. A. Understanding Artifacts in Impedance Spectroscopy. *J. Electrochem. Soc.* **162**, H47–H57 (2014).

34. Schiefelbein, S. L. A new technique to measure the electrical properties of molten oxides. (Massachusetts Institute of Technology, 1996).

35. Schellinger, A. K. & Olsen, R. P. The relationship between electrical conductivity and composition of molten lead silicate slags. *JOM* **1**, 984–986 (1949).

36. Bockris, J. O. & Mellors, G. W. Electric Transport in Liquid Lead Silicates and Borates. *J. Phys. Chem.* **60**, 1321–1328 (1956).

37. Ito, H. & Yanagase, T. Studies on Lead Silicate Melts. *Trans. Japan Inst. Met.* **1**, 115–120 (1960).

38. Suginohara, Y., Yanagase, T. & Ito, H. The Effects of Oxide Additions upon the Structure Sensitive Properties of Lead Silicate Melts. *Trans. Japan Inst. Met.* **3**, 227–233 (1962).

39. Ejima, T., Watanabe, Y. & Kameda, M. Electric Conductance in the Liquid PbO-SiO2 Binary System (Electric Conductance in Liquid Lead Silicates(I)). *J. Japan Inst. Met. Japan Inst. Met. Mater.* **32**, 1250–1256 (1968).

40. Ashizuka, M. & Ohtani, M. The Measurement of the Electrical Conductivity of Silicate Melts Containing PbO and Na2O. *J. Japan Inst. Met. Japan Inst. Met. Mater.* **33**, 498–503 (1969).

41. SAITO H, GOTO K & SOMENO M. Electric Conductivity of Liquid Pbo-Sio2, Pbo- Geo2, Pbo- P2O5, Pbo-B2O3 and Pbo- Sio2- Geo2 System. *Iron Steel Inst Japan-J* **55**, 539–549 (1969).

42. Kawahara, M., Morinaga, K. & Yanagase, T. The Behavior of MgO and NiO in Molten PbO-SiO2 System. *J. Japan Inst. Met.* **43**, 309–315 (1979).

43. Pal, U., Debroy, T. & Simkovich, G. Electronic and ionic transport in liquid PbO-SiO2 systems. *Metall. Trans. B* **16**, 77–82 (1985).

44. Bockris, J. O. M., Kitchener, J. A., Ignatowicz, S. & Tomlinson, J. W. Electric conductance in liquid silicates. *Trans. Faraday Soc.* **48**, 75–91 (1952).

45. Cnockaert, V. *et al.* Determination of the Fe3+/ Σ Fe Ratio in Synthetic Lead Silicate Slags Using X-Band CW-EPR. *J. Sustain. Metall.* **7**, 519–536 (2021).

46. Bale, C. W. *et al.* FactSage thermochemical software and databases, 2010-2016. *Calphad Comput. Coupling Phase Diagrams Thermochem.* **54**, 35–53 (2016).

47. Allibert, M. & Eisenhüttenleute, V. D. *Slag atlas*. *TA - TT* - (Verlag Stahleisen, 1995). doi:LK - https://worldcat.org/title/36859350.

Figures

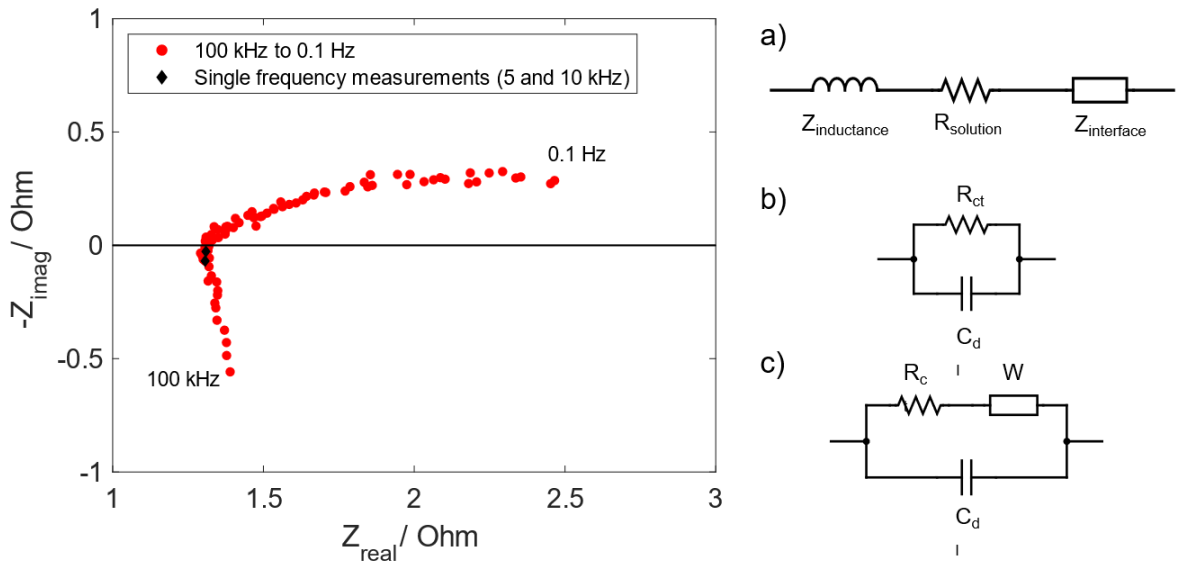

Figure 1. Nyquist plot for a binary SiO_2-PbO slag at 1200 °C. The impedance was measured galvanostatically between 100 kHz and 0.1 Hz with an excitation current of 100 µA. Circuit a) represents a general equivalent circuit for interpreting the Nyquist plot. Circuits b) and c) represent equivalent circuits that are used to represent $Z_{interface}$.

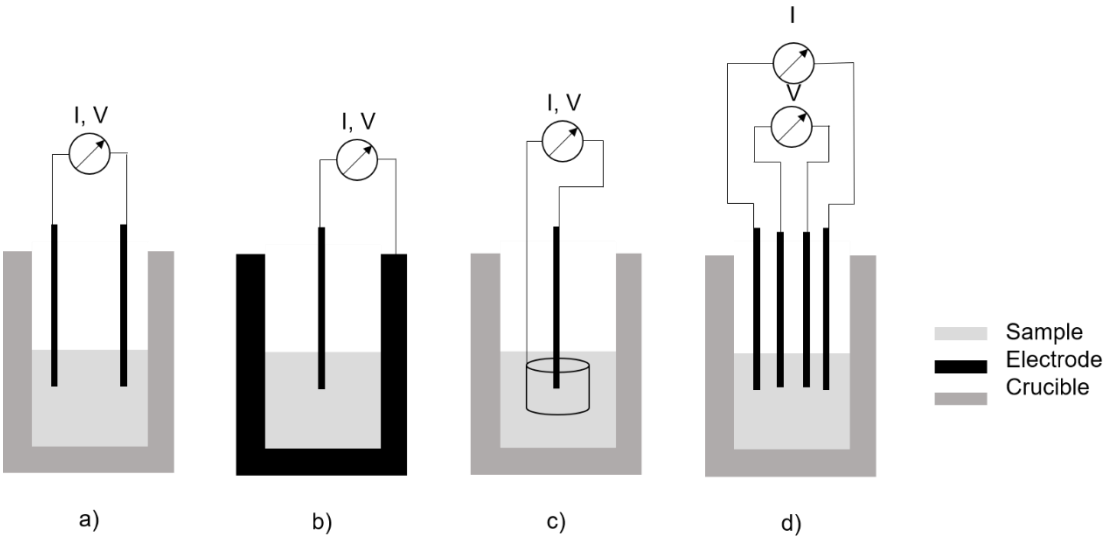

Figure 2 Overview of different configurations for electrical conductivity measurements. a) two-electrode, b) central electrode, c) ring electrode and d) four-electrode. Adapted from Zhang et al.[6]

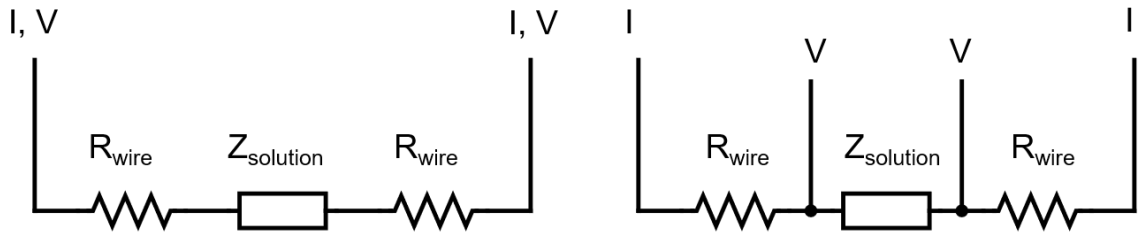

Figure 3. Circuit associated with a two-electrode configuration (left) and a four-electrode configuration (right). Since the current and voltage are measured at the same electrodes in the two-electrode setup, the resistance of the wires is included in the impedance measurements. The four-electrode configuration manages to isolate the solution impedance from the wire resistances though.

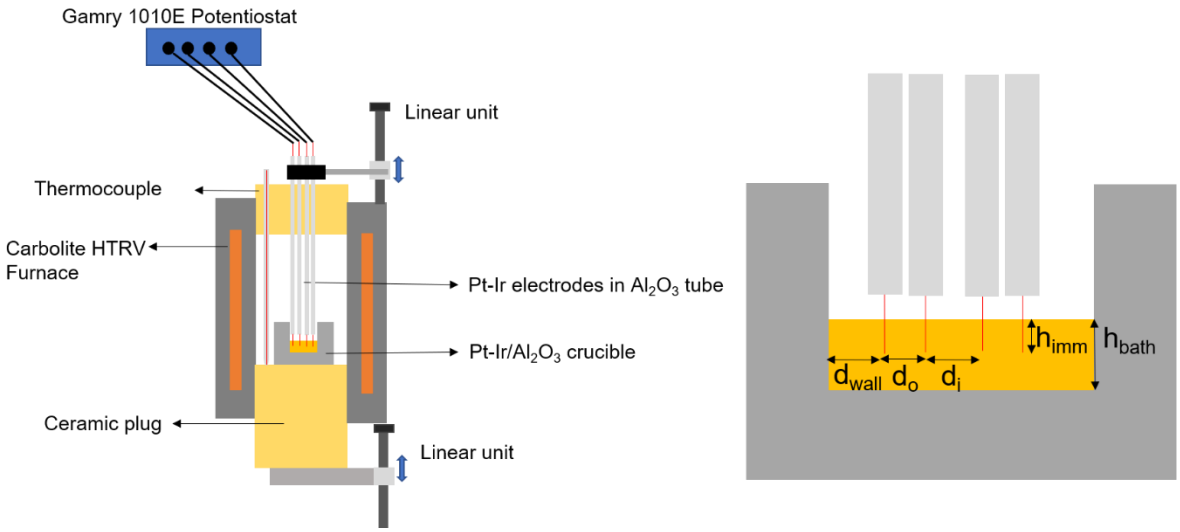

Figure 4. Schematic overview of the constructed setup and close-up of the crucible and electrode geometry.

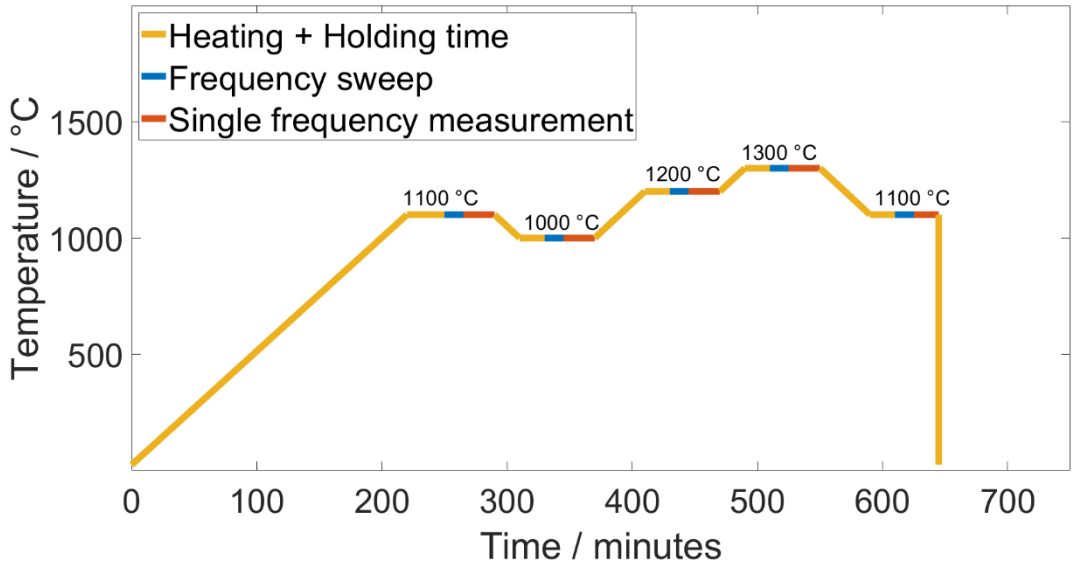

Figure 5. Temperature profile and corresponding measurement scheme of the high temperature measurements. The conductivity was measured twice at 1100 °C to make an estimation of the error due to PbO evaporation along the experimental run.

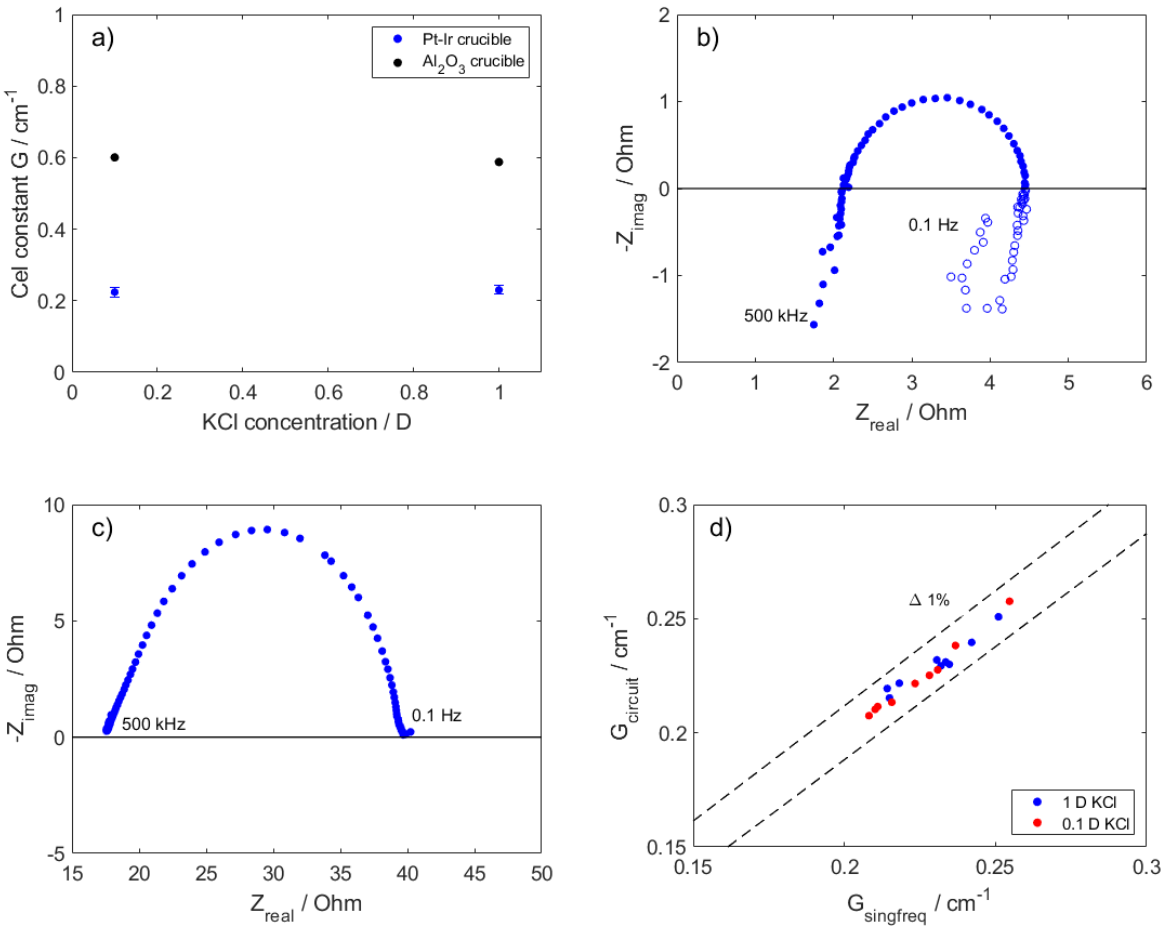

Figure 6. a) Average cell constant G (cm^{-1}) as a function of the KCl concentration of the aqueous calibration solution. 6. b) and 6. c) example of Nyquist plots for respectively the 1 D and 0.1 D KCl solution and the corresponding equivalent circuits. Open circles are excluded for the determination of the equivalent circuit parameters as these are considered to be a measurement artefact of the four-electrode setup. 6. d) compares the cell constant from the single frequency measurements $G_{singfreq}$ with the one from the circuit fit measurement $G_{circuit}$.

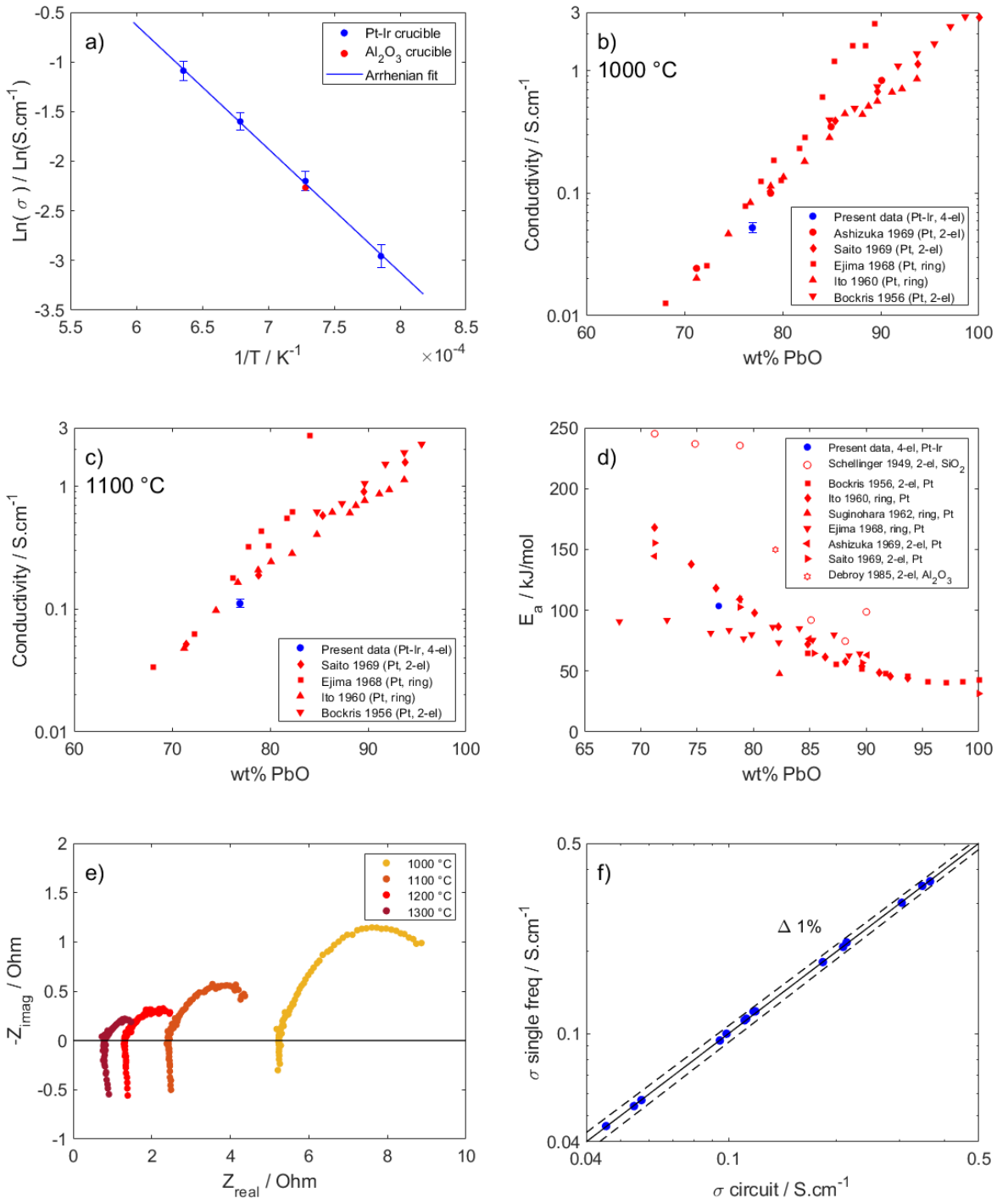

Figure 7. a) Natural logarithm of the electrical conductivity (S/cm) as a function of the reciprocal of the temperature for measurements in a Pt-Ir (blue) and Al_2O_3 (red) crucible. The blue data points were fitted to an Arrhenian function as well. b) and c) comparison of our data with literature for 1000 °C and 1100 °C as a function of the composition. d) comparison of the obtained activation energy with literature. e) Nyquist plots for varying frequencies of 100 kHz to 0.1 Hz obtained as a function of temperature. f) Comparison of the electrical conductivity obtained via the single frequency method and EIS.

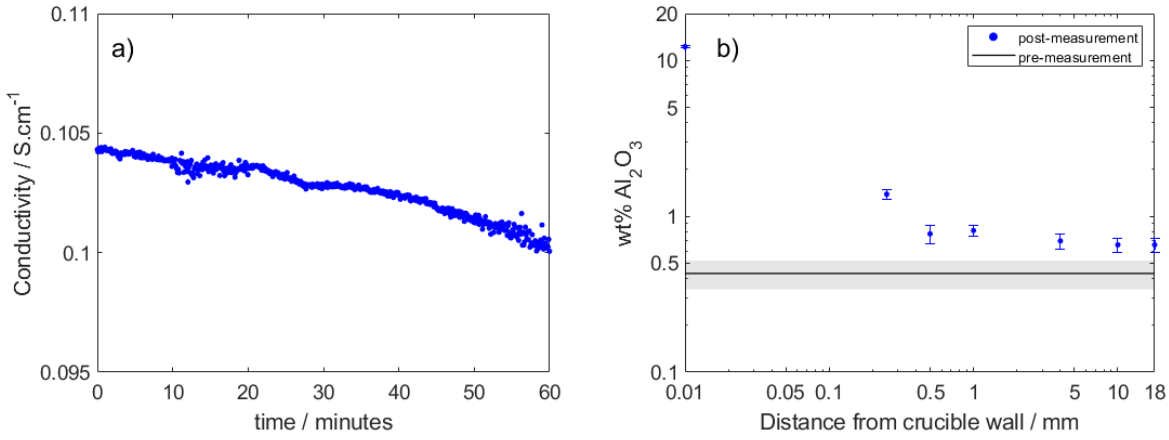

Figure 8. a) Electrical conductivity at 1100 °C as a function of the measurement time when using an Al_2O_3 crucible which shows a continuous decrease. b) wt% Al_2O_3 as a function of the distance from the crucible obtained via SEM-EDX. Measurements were taken at a depth of 3 mm from the slag surface, measured from the center of the crucible. The first measurement (at 0.01 mm) was taken at the crucible-slag interface. The grey are indicates the standard deviation on the wt% Al_2O_3 of the original composition.